Field Measurements and Comparisons to Simulations of High Energy Laser Propagation and Off-Axis Scatter

Conference Paper *in* Proceedings of SPIE - The International Society for Optical Engineering · August 2010

DOI: 10.1117/12.860046

6 authors, including:

Steven Fiorino
Air Force Institute of Technology

Robb M. Randall
AtmoFX LLC (Atmospheric and Climate Effects Consulting)

Richard Bartell
Intregrity Appplications Inc

John Haiducek
University of Michigan

Field measurements and comparisons to simulations of high energy laser propagation and off-axis scatter

Steven Fiorino, Robb Randall, Richard Bartell, John Haiducek, Mark Spencer, et al.

Steven T. Fiorino, Robb M. Randall, Richard J. Bartell, John D. Haiducek, Mark F. Spencer, Salvatore J. Cusumano, "Field measurements and comparisons to simulations of high energy laser propagation and off-axis scatter," Proc. SPIE 7814, Free-Space Laser Communications X, 78140P (24 August 2010); doi: 10.1117/12.860046

Event: SPIE Optical Engineering + Applications, 2010, San Diego, California, United States

Field Measurements and Comparisons to Simulations of High Energy Laser Propagation and Off-Axis Scatter

Steven T. Fiorino, Robb M. Randall, Richard J. Bartell, John D. Haiducek,
Mark F. Spencer and Salvatore J. Cusumano

Air Force Institute of Technology
Center for Directed Energy
2950 Hobson Way
Wright-Patterson AFB, OH 45433-7765

ABSTRACT

The AFIT Center for Directed Energy's High Energy Laser End-to-End Operational Simulation (HELEEOS) model allows for the calculation of the irradiance from within a high energy laser beam that is scattered by molecules and particulates in the atmosphere to an off-axis observation point, while incorporating the spreading effects of the turbulence and thermal blooming. Field experiments conducted at Wright-Patterson AFB, Ohio in summer 2009 allowed for validation measurements for the HELEEOS off-axis algorithm to be collected. Turbulence strength measurements were made at a wavelength of 1.55 μm using a state of the art bistatic turbulence profiler for both horizontal and vertical paths. Pressure, wind speed, wind direction, relative humidity and aerosol loading data were collected simultaneously with the C_n^2 measurements. As part of the experiment, the profiler's beams were imaged off-axis with a calibrated camera array and the received irradiance of the off-axis scattering was quantified. Characterization of the aerosol distribution along the laser path and the path to the observer is accomplished by determining the visibility and climatological aerosols for southwestern Ohio. Comparisons between predicted and measured off-axis irradiance are made.

Keywords: HELEEOS, high energy laser, atmospheric scattering

INTRODUCTION

HELEEOS is a software package developed at AFIT to simulate laser propagation through the atmosphere[1]. Its core purpose is to predict the properties of a high energy laser beam at every point along its path, taking into account its interaction with the atmosphere[2]. In 2006, AFIT master's student Scott Belton extended the model to simulate off-axis scattering, giving HELEEOS the ability to determine the scattered irradiance of a laser at some off-axis location[3]. Although HELEEOS's basic functionality has been experimentally validated, the off-axis scattering capability has not previously been validated. Tests with an infrared camera and 1 to 5-watt infrared lasers at Wright-Patterson Air Force Base provide a means to determine the accuracy of the off-axis scattering model. The model was designed with high-energy laser weapons in mind, but these tests provide useful data for validation purposes, as well as to determine the viability of using the same model for lower power communication lasers. Future tests to be conducted by the Naval Research Laboratory in Dahlgren, VA will provide a means to validate the model against a high energy laser.

1.1 Background

Lasers are operated in the atmosphere for a variety of military applications, including illumination of targets for bombs and missiles, communication, and most recently as experimental directed-energy weapons. The Air Force has built two

*steven.fiorino@afit.edu; phone 937 255 3636 x4506; fax 937 656 6000; www.afit.edu

Free-Space Laser Communications X, edited by Arun K. Majumdar, Christopher C. Davis,
Proc. of SPIE Vol. 7814, 78140P · © 2010 SPIE · CCC code: 0277-786X/10/$18 · doi: 10.1117/12.860046

experimental laser weapons, the Airborne Laser (ABL) and the Advanced Tactical Laser (ATL). Both use Chemical Oxygen Iodine (COIL) lasers. The ATL is carried inside a modified C-130 aircraft and is designed to melt through targets along slant paths up to up to 10 km. The ABL, on the other hand, is intended for use against theater ballistic missiles such as the SCUD, and would be operated from a modified Boeing 747 aircraft.[4,5] As high-powered lasers become more common, U.S. government agencies will require information about lasers used by our adversaries. Atmospheric scattering makes it possible to observe a laser beam from an off-axis point (i.e. not in the immediate path of the beam), opening the possibility of characterizing the laser by remote observation. Molecules and aerosol particles cause light to be scattered out of the beam in all directions. If the location of the laser, its target, and the observer's location are known, and the atmospheric environment sufficiently well characterized, the power of the laser can be determined from the intensity of the light scattered toward the observer. It may also be possible to use the same technique on some communications lasers. A computer program, written by Belton and since integrated into HELEEOS, provides the computational tools to determine off-axis scattered intensity for a laser of known properties[3].

1.2 Equations for off-axis calculations

The HELEEOS off-axis irradiance calculations can be applied to the scattering effects of molecules, aerosol particles, and hydrometeor particles such as liquid and ice clouds and precipitation. Molecular, aerosol, and hydrometeor scattering remove intensity from the beam. There are primarily two types of scattering that can take place, Rayleigh scattering and Mie scattering. Rayleigh scattering occurs when the wavelength of the beam is smaller than the radius of the particle and Mie scattering occurs when the wavelength of the beam is just about equal to or larger than the radius of the particle. Mie scattering takes place when the size parameter is between 0.2 and 200, while Rayleigh scattering takes place when the size parameter is between 0.002 and 0.2. The size parameter is defined as

$$\chi \equiv \frac{2\pi r}{\lambda} \tag{1}$$

where r is the radius of the particle and λ is the wavelength of the beam. As the size parameter increases the amount of forward scattering increases as well. This occurs whether the particle has spherical shape or not[6].

The scattering function angle will be the major factor. The equation in HELEEOS that calculates this value is as follows,

$$\frac{P(\theta)}{4\pi} = \frac{\lambda^2}{4\pi^2} \sum_{i=r_{\min}}^{r_{\max}} n(r) \frac{i_1 + i_2}{2} \Delta r_i \tag{2}$$

where λ is the wavelength of the beam, $n(r)$ is the particle size distribution, $i_1 = S_1 S_1'$, $i_2 = S_2 S_2'$, and S_1 and S_2 are intensity functions. This determines the angle from the original axis of propagation at which photos are scattered. The scattering phase function is used to calculate how much laser energy is scattered in any off-axis direction. Figure 1 is an example of HELEEOS-calculated phase functions for energy at 550 nm in scattering volumes dominated by molecules, aerosols, or clouds and rain hydrometeors.

In HELEEOS, the single scatter of a photon is calculated. Single scattering—when a photon is redirected only once as it traverses a medium—applies when the scattering medium is relatively thin. Multiple scattering is when a photon is scattered more than once as it passes through a medium; this can be computationally expensive to calculate. In dense scattering mediums (such as visible light in clouds) photons can be scattered millions of times in all directions, causing some photons to scatter back into the original axis of the laser beam or energy path. The current HELEEOS off-axis algorithm does not take into account multiple scattering since high energy laser engagements are expected to occur away from highly scattering environments. Adding scattering and absorption together gives a total, which is called extinction. Extinction is the amount of a laser beam that is not reaching its intended destination along the original axis. Transmission is the ratio of the initial transmitted energy or intensity over the received amount of energy or intensity. Transmission is a value between 0 and 1.

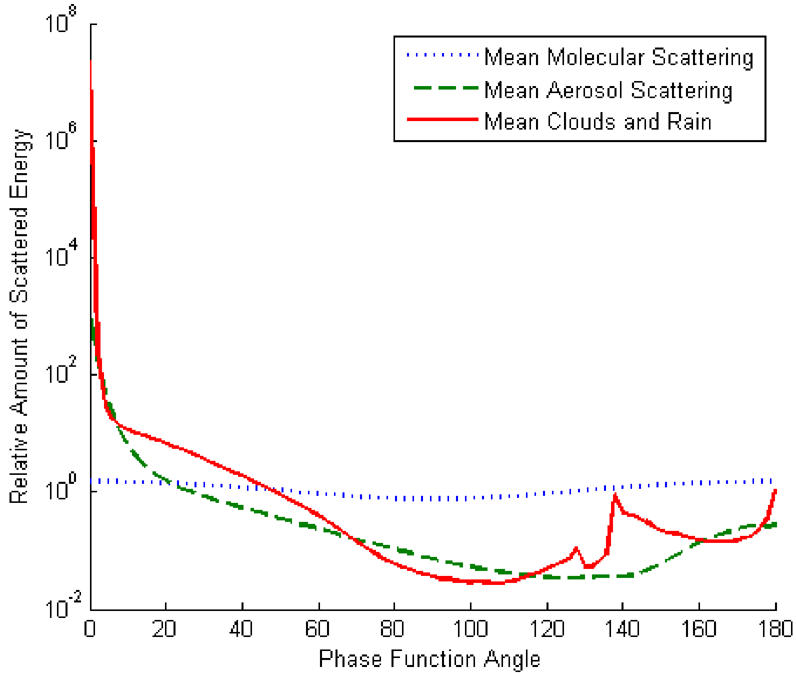

Fig 1: Example HELEEOS-calculated phase functions at 0.55 µm for air molecules, a typical distribution of midlatitude aerosols, and a combined distribution of cloud droplets and rain drops.

The amount of scattered intensity that reaches the off-axis observing point can be described using scattered amplitude or phase. Following Stephens[7], the equation,

$$I_{SCA} = \frac{\left|S(\Theta)\right|^2 I_o}{k^2 R^2} \tag{3}$$

relates amplitude function *S(Θ)* (described as a scattering pattern) and initial beam intensity I_o to scattered off-axis intensity. The next equation,

$$\frac{1}{4\pi} P(\Theta) = \frac{\left|S(\Theta)\right|^2}{k^2 C_{SCA}} \tag{4}$$

relates the scattering phase function $P(\Theta)$ to amplitude function[7]. Combining these two equations gives the equation,

$$I_{SCA} = \frac{P(\Theta) C_{SCA} I_O}{4\pi R^2} \tag{5}$$

where C_{SCA} is the scattering cross section (dimensions of area) of the scattering particle, I_O is the initial incident intensity of the scattering particle, and R is the distance between the receiver and the beam. Typically scattering cross section has the units of m^2, scattered intensity has the units of $Wm^{-2}Sr^{-1}$, R has the units of m, and the phase function is dimensionless. This equation allows the scattered intensity to be calculated from the phase angle, which is an output of the Wiscombe[8] Mie scattering module within HELEEOS. Unfortunately, Equation 5 only yields the scattered intensity due to of one particle at the off-axis point. Therefore the scattering particle number density N (per unit volume) is needed to account for the scattered intensity due to a distribution of particles. Since the scattering cross section is equal to the volume scattering coefficient divided by the number density, multiplying by the number density N would cause the number densities on top and bottom to cancel out leaving just the volume scattering coefficient β_{SCA} (units of inverse length). The scattering cross-section is related to β_{SCA} via:

$$C_{SCA} = \frac{\beta_{SCA}}{N} \tag{6}$$

Combining Equations 5 and 6 yields the scattered intensity as a function of scattering angle and volume scattering coefficient

$$I_{SCA} = \frac{P(\Theta)\beta_{SCA} I_O}{4\pi R^2} dv \tag{7}$$

where *dv* is the scattering volume.

Currently, the way HELEEOS analyzes laser beams is by splitting the beam up into 1,000 different segments. In the initial testing of the algorithm, the beam was broken down into only 100 segments to reduce computational expense. The intensity being scattered onto the off-axis receiver of each one of these segments is calculated separately and then added to give the total scattered irradiance. Ultimately, the equation of scattered irradiance becomes,

$$I_{SCA} = \sum_{i=1}^{100} \frac{P(\Theta)_i \beta_{SCAi} I_{Oi}}{4\pi R_i^2} dv_i \tag{8}$$

Each one of the segments being analyzed has a different phase angle $P(\Theta)_i$. A few calculations are necessary to compute these angles. Referring to Figure 2 below, the equation of Line B is found from the platform to the target using the equation of a line. Next, the distance from the point where the off-axis receiver is to line B is found (labeled as distance R). The equation of this line must also be found, which is represented as line A in the figure. Line A is orthogonal to Line B, so the dot product of these two lines is equal to zero. The point where Line A and Line B intersect is calculated and this is called point P1. The distance from point P1 to the platform is represented as D1 and the distance from point P1 to the target is represented as D2. The phase angle for each of the segments of the beam that are between point P1 and the platform is calculated using the standard arctangent function.

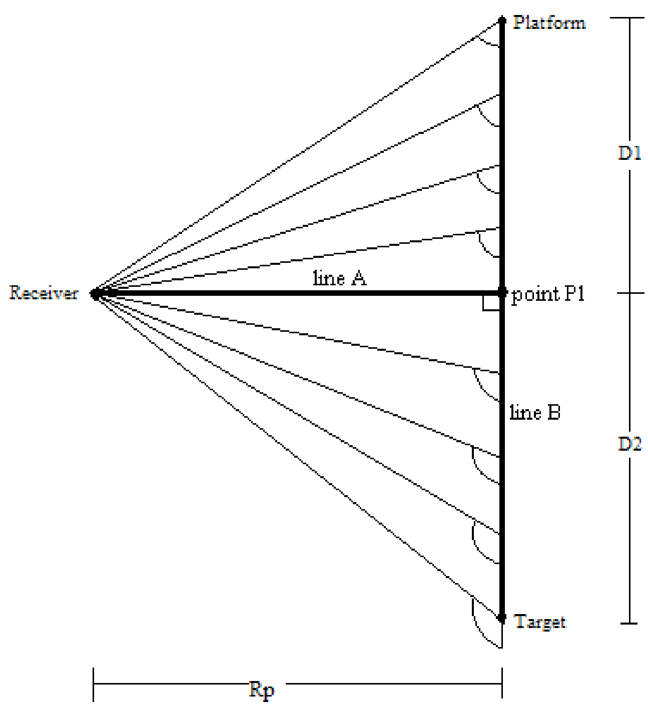

Fig 2: Schematic example of the HELEEOS geometric set-up for observed off-axis irradiance and the breakdown of the total beam into segments for analysis.

One last factor must be taken into consideration when calculating the scattered intensity at an off-axis point. Equation 8 does not include extinction to the off-axis observation point. The final addition this equation needs is to include the transmittance from each of the scattering beam segments to the off-axis observer. Transmittance is already a value that HELEEOS computes, and with the off-axis algorithm invoked, it will calculate all the individual off-axis transmittances. The way that HELEEOS computes this transmittance is by simulating a laser beam from a platform to a target and calculating the amount of irradiance reaching the target. The current control-script for this research written uses HELEEOS to calculate the transmittance by simulating a laser beam from the segment being analyzed to the off-axis point. Each segment of the beam that is being analyzed is a different distance away from the observer and has a different transmittance value. This is because atmospheric transmittance decreases with altitude, and each segment can be at a different altitude. The scattered, off-axis intensity is then multiplied by the transmittance value that HELEEOS generates. The end equation is

$$I_{SCA} = \sum_{i=1}^{100} \frac{P(\Theta)_i \beta_{SCAi} I_{Oi} t_i}{4\pi R_i^2} dv_i \tag{9}$$

where *t is* transmittance. The transmittance equation is,

$$t(s_1, s_2) \equiv e^{-\int_{S_1}^{S_2} \beta_{ext} dx} \approx e^{-\beta_{ext} \cdot R} \tag{10}$$

where S_1 is the beginning of the optical path and S_2 is the end of the optical path being calculated and β_{ext} considers both absorption and scattering of the scattered off-axis intensity.

2. OFF-AXIS ANALYSIS PROCESS

2.1 Camera calibration

The camera, a XenICs Xeva 409, was calibrated against a CI Systems SR80-12HT blackbody at a variety of temperatures between 200 and 500 ºC, with the camera placed at a distance of 600 cm[10]. The camera viewed the blackbody through a telescope having a 10.10 cm aperture, the smaller of the two telescopes used in field observations. A band-pass filter was placed in front of the telescope, which has a pass band extending from 1.49 µm to 1.62 µm. The field of view of telescope-camera combination was sufficiently small that the 12-inch blackbody over-filled the detector's field of view. The larger of the two telescopes, a reflecting telescope with a 31.75 cm aperture, needed to be much farther away from its target in order to focus, and adequate space was not available in the laboratory. Therefore the calibration results for the smaller telescope had to be applied to images collected with the larger telescope as well. This was possible to do because the same camera was moved back and forth between the two telescopes.

A number of images of the blackbody were collected, and multiple linear regression was used to determine a function

$$\Phi_{px} = A + B(V_{px}) + C(\tau_{\text{int}}) \tag{11}$$

mapping the flux Φ_{px} for each pixel to the camera output V_{px} and the integration time τ_{int}. The fluxes Φ_{px} were computed using Planck theory. Although camera calibrations normally do not account for integration times, this additional term greatly improved the quality of the fit.

2.2 Background subtraction

Most of the field images consist of laser scatter in front of background scenery. Many of these show the laser turning on or off, in which case the background can be computed as the average of some of the frames in which the laser is turned off. Subtracting this average from a frame in which the laser is on yields an image in which most pixels have values near zero, except for those containing laser beam scatter. Unfortunately, the background fluctuates slightly with time, due to variances in solar illumination (due to passing clouds) or other factors. In order to eliminate this bias, a histogram is computed from the image being studied. Since most of the pixels are background pixels, the maximum of the histogram indicates the overall shift in background compared with the previously-computed average. Subtracting this maximum value from the entire image will remove most of the temporal variance in the background. Much of the background contains noise which cannot be eliminated. After shifting the background, however, the noise has an average value of zero, so that positive noise will, on average, cancel out negative noise when a sum is computed over a region of the image.

2.3 Relating camera irradiances to HELEEOS outputs

In analyzing the data, it is necessary to relate pixels in the scene to physical locations in the experiment. In order to do this, the geometry relevant to each pixel is considered relative to the source and observer as shown in Figure 3. The location of a pixel along the laser beam path is described relative to the source in the form of the distance BD, and relative to the observer in terms of the angle *a*, called the observer angle. In order to determine the distance BD from the angle *a*, or vice versa, the off-axis angle *b* and the distance AB must be known.

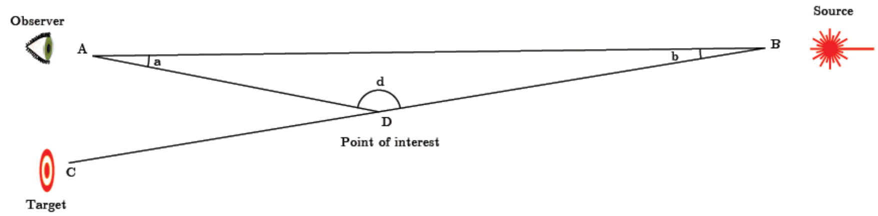

Fig 3: Experiment setup with a triangle shown between the observer, source, and a point of interest along the laser beam path.

The HELEEOS off-axis scattering model requires a specific point or range of points along the length of the beam at which to compute the scattering toward the observer. In order to obtain verifiable output, this range of points must be matched to pixels in the camera image. If off-axis angle *b* is known, as well as the distance AB, then the angle *a* and the distance BD can be related to each other trigonometrically.

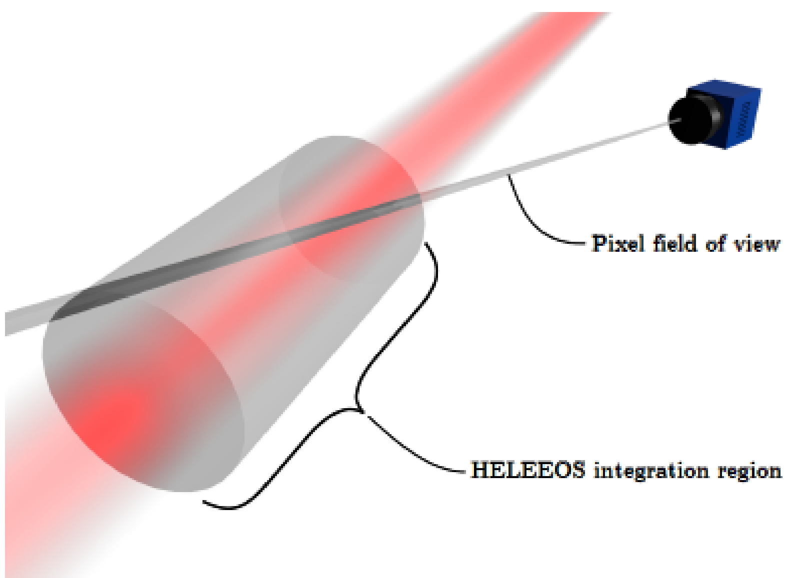

Fig 4: HELEEOS computes the total irradiance from a cylindrical length of the beam, while each pixel of an image records the total irradiance scattered from points in its field of view. To compare the two, irradiances from multiple pixels must be combined such that they contain the cylindrical region being integrated in HELEEOS.

To obtain a single irradiance value for each image which can be related to a HELEEOS output, a region in the image is selected to correspond to a range of distances along the beam, and irradiances for all the pixels in this region are added together to obtain a total irradiance for the image as shown in Figure 4.

3. FIELD MEASUREMENTS

Field measurements were taken of a laser test conducted at Wright-Patterson Air Force Base Area B in July, 2009. Most of the available movies showed atmospheric scattering. Irradiance values were computed from these images and compared to HELEEOS output.

3.1 Experiment geometry

The 15 July 2009 test was conducted with a source laser at the west end of the abandoned runway at Area B of WPAFB, with the target on the ninth floor of Building 622[9]. The total distance from source to target was approximately 3050 m. The observer was located on a concrete pad on the west side of the parking lot at Building 622, approximately 60 m from the target and 3015 m from the source. The distance from observer to target was measured using a laser rangefinder; all other distances were measured using Google Earth. This setup is shown in Figure 5. The source was located at an elevation of 240 m, while the target was at 313 m. The observer was located at an elevation of 292 m. The elevation and altitude differences altogether place the observation location approximately 0.9 degrees off-axis.

For the 17 July 2009 test, the source laser was located near the east end of the abandoned runway at Area B of WPAFB, with the target 2160 meters away at the west end of the runway. Off-axis scattering was observed from a location roughly 46 meters from the target in a direction perpendicular to the beam path. Thus the observer location is around 1.22 degrees off-axis. This setup is shown in Figure 6. The relevant distances were measured using a laser rangefinder. Observer, source, and target were all located at roughly the same elevation of 240 m.

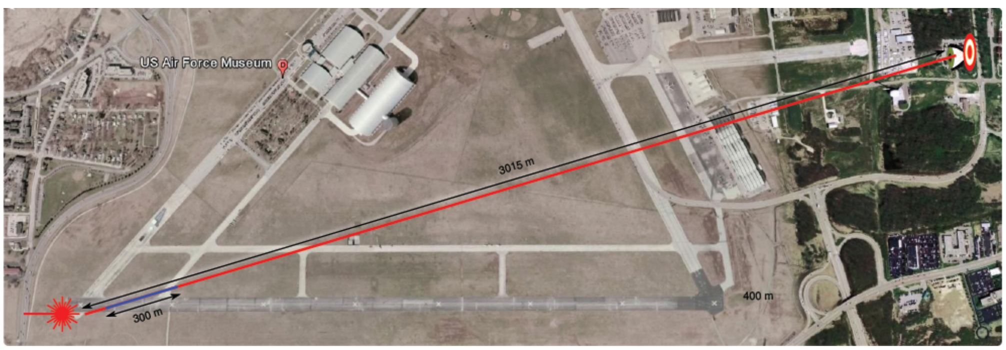

Fig 5: Experiment geometry for the 15 July 2009 test. For this test, the observer was located almost directly below the beam. The 300 m field of view is representative of the 31.75 cm reflecting telescope, which was used for most of the observations on 15 July. results

Fig. 6: Experiment geometry for the 17 July 2009 test. The source is denoted by a laser symbol, the target by a bulls-eye, and the observer by an eyeball. The observer's field of view is identified by a blue line along the laser beam path. The 400 m field of view is representative of the 10.1 cm refracting telescope, which was used for most of the observations on 17 July.

During the course of the experiment the lasers were sometimes walked off from the target, but the precise direction of the walk-off was not determined. Therefore, in computing the observer's off-axis angle it is assumed that the lasers are always pointed at the intended target. This off-axis angle is used both in determining the observation path and as an input parameter to HELEEOS.

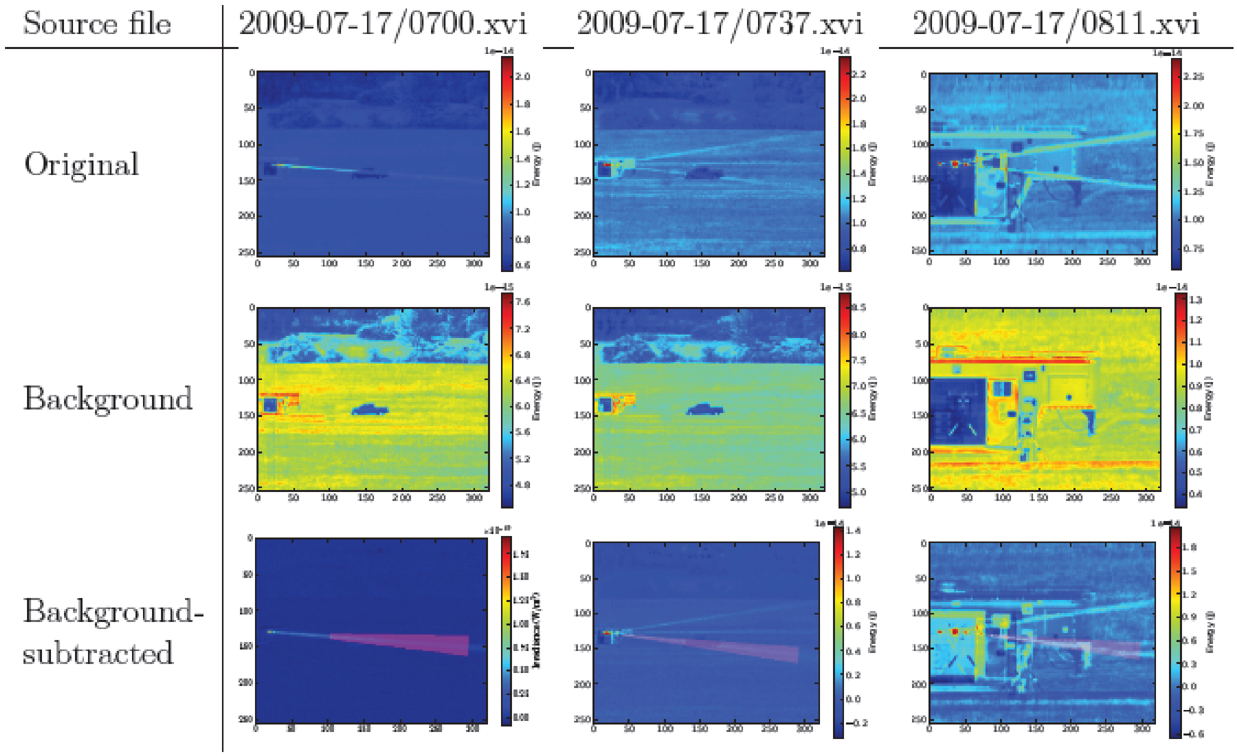

Fig. 7: Examples of background subtraction[10].

3.2 Image Selection

In order for a data collection to be used, atmospheric scattering must be visible in the images, and it must be possible to determine which of the lasers is responsible for the scattering. In addition, it must be possible to determine the physical location of the beam from image coordinates. In order to do this, images were selected in which the laser source was visible in the picture and in which the camera was stationary. Finally, a background image must be available. Ideally this can be created from an average of frames in the same data set. For instance, if the movie shows the lasers being turned on or off it will often include a substantial number of frames in which no lasers are turned on. Otherwise, a background image can be constructed from another image of the same scene. When the background was constructed from another image, the result was generally inferior, but images processed in this way were kept since they did not consistently appear as outliers in the final data set.

The quality of the images used varied significantly. Most notable was the varying effectiveness of the background subtraction technique. The best results occurred when the background could be computed from different frames of the same file, while subtracting a background computed from a different file yielded far poorer results. Examples of the background subtraction results are shown in Figure 7.

The left-hand column of Figure 7 shows a highly successful background subtraction. The resulting image contains near-zero values almost everywhere except where the laser beam can be seen. The center column shows a moderately successful background subtraction. In this image, background features remain visible in the image after background subtraction has been performed, but the laser beam pixels generally contain much larger magnitudes than do background pixels.

The right-hand column of Figure 7 shows a relatively unsuccessful background subtraction. Many background features have magnitudes at or above those of the laser beam pixels, even after background subtraction. Still, the irradiances computed for these images did not tend to be outliers when compared with those computed from other images. As a result, less successful cases of background subtraction were included in the final data set.

3.3 Off-Axis Results

In total the calibration was applied to 56 images taken at the July 2009 laser test. For each image, an irradiance value was computed using HELEEOS and compared with that measured from the image. The results of this analysis can be seen in Figure 8. HELEEOS outputs correlate weakly to measured irradiances. In many cases the HELEEOS outputs came within an order of magnitude of the measurements, with the worst cases being off by two orders of magnitude.

In nearly all of the field images it is apparent that irradiance decays along the length of the beam. Figure 9 shows an example of this. The selection region of Figure 9 has been divided into segments in order to quantify the downward trend in irradiance. Each segment corresponds to a relatively narrow range of angles in the observer's field of view, and the irradiance can be computed for each segment as shown in Figure 10. HELEEOS often predicts significantly different irradiances and a different rate of decay as a function of angle, but the overall downward trend as a function of angle is present in the HELEEOS output.

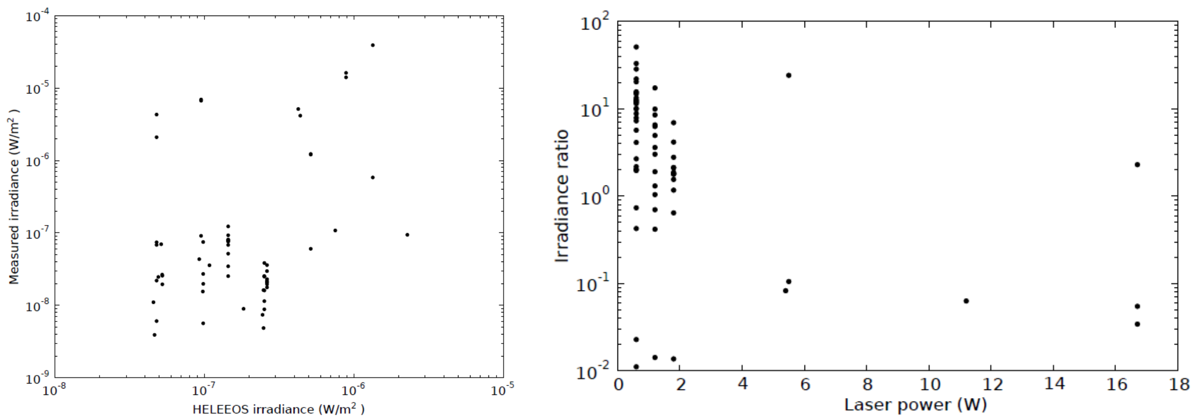

Fig. 8: Comparison of HELEEOS-derived irradiances with measured irradiances, showing a weak correlation. The plot on the left shows the weak correlation between measured irradiance and HELEEOS output; the plot on the right shows the ratio of the two as a function of laser power[10].

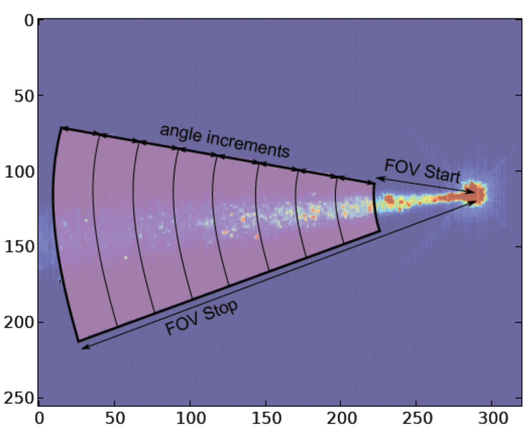

Fig. 9: Angle increments within the selected field of view, used for computing irradiances as a function of viewing angle[10].

At more extreme angles (45-90º) the beam became too faint for the camera to detect. At these angles it was impossible to measure the irradiance, but the inability to detect the beam indicates that the irradiance should be much lower than at the small angles used in Figure 10. A succession of HELEEOS runs using greater angles revealed that HELEEOS continues to produce lower irradiances through a 75º viewing angle, consistent with the fact that the scatter could not be detected at that angle.

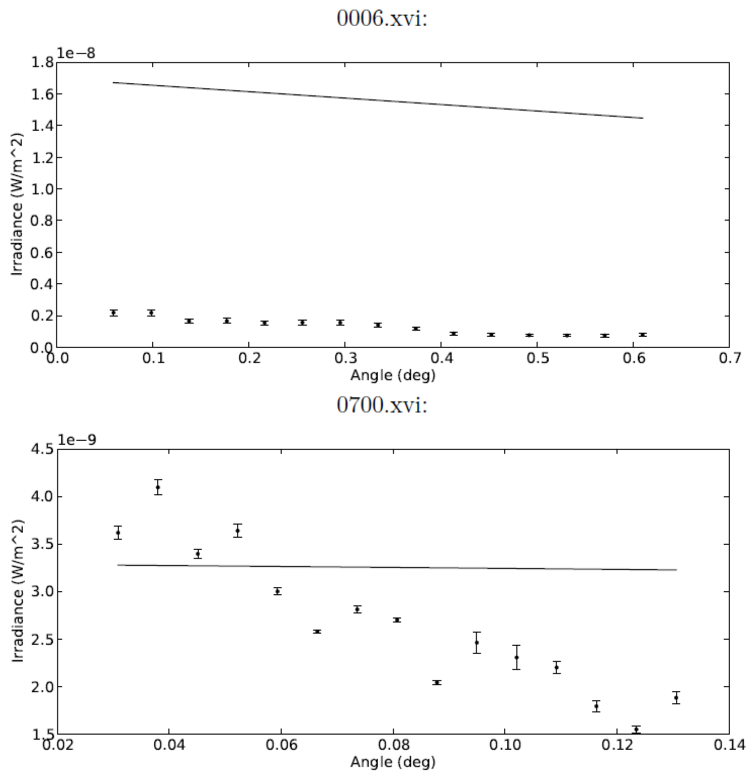

Fig. 10: HELEEOS-predicted irradiance (solid lines) and measured irradiance (points) as a function of observation direction for two images. The error bars are computed as the standard deviation of the irradiance over all the animation frames used. Although the overall magnitude differs between HELEEOS and the measured irradiance, as does the rate at which the irradiance falls off with distance, the downward trend is present in both[10].

4. CONCLUSIONS

The tests conducted in this research show some agreement between HELEEOS-predicted off-axis irradiances and those measured using a camera. The data were not in close enough agreement with HELEEOS to serve as a validation of HELEEOS by themselves, but HELEEOS showed some correlation with the test data in terms of laser power output and viewing angle. For the entire set of test data, HELEEOS produced outputs within two orders of magnitude, and frequently within one order of magnitude. Although these errors are large, there are cases in which precision such as this would be adequate. For instance, if one wished to determine whether a certain laser could be detected under a particular set of conditions, one could use HELEEOS to do this. As long as HELEEOS predicted irradiances more than two orders of magnitude above or below the threshold for detection, one could make a fairly certain determination as to whether the laser could be detected under those conditions. For a laser weapon, a two order of magnitude accuracy would in certain cases be sufficient to determine whether a laser was capable of destroying a particular target.

Although the two order of magnitude threshold sets an upper bound on the uncertainty of HELEEOS results for this set of operating conditions (clear air, 1.5-1.6 μm, 0.6-5.7 W, and camera roughly 1º off axis), the real value of this test is to demonstrate techniques for collecting and analyzing off-axis scattering data, and to provide insights into the best path toward validating HELEEOS. The test showed that an infrared camera can be used successfully to measure off-axis scattering data, and techniques were developed that can be used to relate that data to HELEEOS inputs and outputs, both for purposes of validation and for later real-world applications. The large discrepancies between HELEEOS outputs and measured irradiances suggest that a sensitivity study of the off-axis scattering model should be accomplished in order to guide further testing.

5. ACKNOWLEDGEMENT

The views expressed in this paper are those of the authors and do not necessarily reflect the official policy or position of the Air Force, the Department of Defense or the U.S. Government.

REFERENCES

[1] Bartell, R.J., G.P. Perram, S.T. Fiorino, S.N. Long, M.J. Houle, C.A. Rice, Z.P. Manning, M.J. Krizo, D.W. Bunch, and L.E. Gravley, "Methodology for Comparing Worldwide Performance of Diverse Weight-Constrained High Energy Laser Systems" *Proc.* SPIE **5792**, 76-87 (2005).

[2] Fiorino, S.T., R.J. Bartell, G.P. Perram, D.W. Bunch, L.E. Gravley, C.A. Rice, Z.P. Manning, and M.J. Krizo, 2006: The HELEEOS atmospheric effects package: A probabilistic method for evaluating uncertainty in low-altitude high energy laser effectiveness *J. Dir. Energy*, **Vol 1**, No. 4, pp. 347-360.

[3] Belton, S. L. "The Simulation of Off- Axis Laser Propagation Using HELEEOS". Master's thesis, Graduate School of Engineering, AFIT/GSS/ENP/06-01, Air Force Institute of Technology (AETC), Wright-Patterson AFB, OH, (2006).

[4] "ABL YAL 1A Airborne Laser, USA", http://www.airforce-technology.com/projects/abl/ (2009).

[5] "Advanced Tactical Laser (ATL)", http://www.globalsecurity.org/military/systems/aircraft/systems/atl.htm, (2005).

[6] Liou, K. N., *An Introduction to Atmospheric Radiation* (Second Ed). Academic Press. 583 pp. (2002).

[7] Stephens, G.L., *Remote Sensing of the Lower Atmosphere*. New York, Oxford, Oxford University Press. 523 pp. (1994).

[8] Wiscombe, W.J., Improved Mie scattering algorithms. *Appl. Opt*., **Vol. 19**(9), 1505-1509. (1980).

[9] Cohen, J.J. "Laser Safety Plan, MZA Long Range Turbulence Profiler - Gen II", (2009).

[10] Haiducek, J.D. "Experimental Validation Techniques for the HELEEOS Off-Axis Laser Propagation Model". Master's thesis, Graduate School of Engineering, AFIT/GAP/ENP/10-07, Air Force Institute of Technology (AETC), Wright-Patterson AFB, OH, (2010).